HYDROLOGICAL PROCESSES
Hydrol. Process. (2013)
Published online in Wiley Online Library
(wileyonlinelibrary.com) DOI: 10.1002/hyp.10068

Regional-scale mapping of groundwater discharge zones using thermal satellite imagery

G. Z. Sass,[1] I. F. Creed,[1]* J. Riddell[2] and S. E. Bayley[3]

[1] *Department of Biology, Western University, London, ON, N6A 5B7, Canada*
[2] *Energy Resources Conservation Board, Alberta Geological Survey, Edmonton, AB T6B 2X3, Canada*
[3] *Department of Biological Sciences, University of Alberta, Edmonton, AB T6G 2E9, Canada*

Abstract:

Mapping groundwater discharge zones at broad spatial scales remains a challenge, particularly in data sparse regions. We applied a regional scale mapping approach based on thermal remote sensing to map discharge zones in a complex watershed with a broad diversity of geological materials, land cover and topographic variation situated within the Prairie Parkland of northern Alberta, Canada. We acquired winter thermal imagery from the USGS Landsat archive to demonstrate the utility of this data source for applications that can complement both scientific and management programs. We showed that the thermally determined potential discharge areas were corroborated with hydrological (spring locations) and chemical (conservative tracers of groundwater) data. This study demonstrates how thermal remote sensing can form part of a comprehensive mapping framework to investigate groundwater resources over broad spatial scales. Copyright © 2013 John Wiley & Sons, Ltd.

KEY WORDS groundwater; discharge; mapping; Landsat; thermal; remote sensing; Prairie Pothole

Received 8 February 2013; Accepted 11 September 2013

INTRODUCTION

Discharge water is found where groundwater flows upwards towards the land surface or where the water table intersects the land surface. A conceptual delineation of discharge *vs* recharge zones was developed in detail by the seminal work of József Tóth in the rolling glaciated terrain of Alberta, Canada (Tóth, 1963, 1971). According to his description, the groundwater regime reflects the combined effects of topography and geology, which together affect the distribution, motion, chemistry and temperature of groundwater (Figure 1). Based on this conceptual model, discharge zones are generally located in topographically low areas that receive groundwater from regional, intermediate and local-scale flow systems and where lakes, rivers or groundwater-fed wetlands often exist. Discharge can occur as point features, such as springs that focus discharge in small areas, or over broad areas, such as riparian areas and seepage faces.

As a result of modified hydrological, biogeochemical and thermal properties of discharge zones, knowledge of their distribution across watersheds and how they connect to the larger hydrological system is essential for understanding ecosystem processes (Brunke and Gonser, 1997) as well as improving freshwater management, regulation and governance (Neufeld, 2000; O'Connor, 2002; Pires, 2004). Areas of active groundwater discharge have important implications for hydrology, as they play an important role in the dynamics of variable source areas and therefore affect runoff processes (Winter *et al.*, 1998). Groundwater discharge not only influences water quantity by providing a steady source of water (baseflow) but it also may influence ecosystems by providing a modified environment through its thermal and chemical signature. The temperature of groundwater discharge zones reflects that of ambient conditions: cooler in the summer and warmer in the winter (Cartwright, 1974). For example, in summer time, groundwater discharge entering streams and lakes provides a cooler environment and thus favour cold water fish like trout (Curry and Noakes, 1995; Power *et al.*, 1999). Discharging groundwater also has a chemical signature that reflects the flowpaths it has traversed often translating to water that has high concentrations of total dissolved solids (TDS), a degree of mineralization proportional to the time the water has spent in the ground (Batelaan *et al.*, 2003; Soulsby *et al.*, 2009). In terms of management, knowing where groundwater discharges onto the surface is important as it contributes to an understanding of the entire flow system which is especially useful to track the movement of contaminants (Whiteman *et al.*, 2012). To meet these scientific and management needs, conceptual and applied approaches are

*Correspondence to: Irena Creed, Department of Biology, Western University, London, ON N6A 5B7, Canada.
E-mail: icreed@uwo.ca

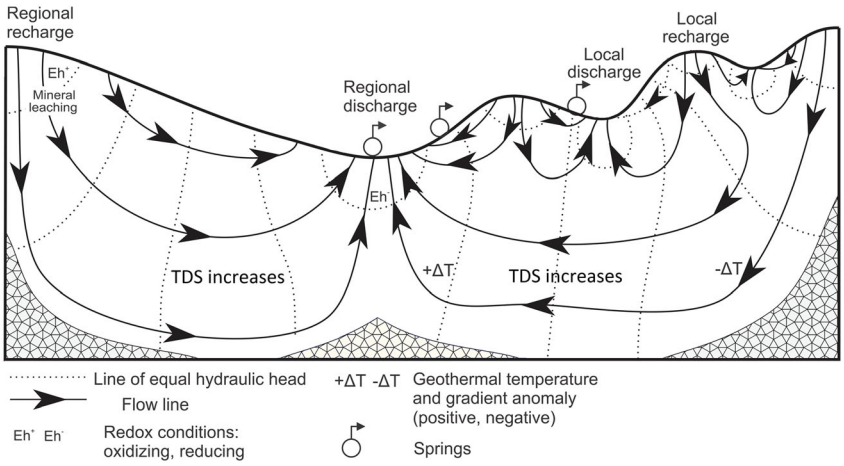

Figure 1. Conceptual understanding of distribution of groundwater recharge and discharge zones and associated chemical and thermal environment (modified from Tóth, 1999)

needed that can be used to delineate the patterns of groundwater discharge zones (Euliss *et al*., 2004).

Turning Tóth's conceptual understanding into accurate maps remains a challenge, especially at regional scales where the traditional method of determining groundwater movement using nests of piezometers and wells becomes prohibitively expensive, impractical and intrusive (Whiteman *et al*., 2012). In places where the geological structure and hydraulic head distribution of a flow system are well characterized, groundwater flow models can be used indirectly to estimate both the magnitude and spatial distribution of groundwater recharge and discharge (Levine and Salvucci, 1999). However, where this information is not well characterized, alternative approaches are needed.

One such alternative that has received a lot of attention is thermal remote sensing (Becker, 2006; Tweed *et al*., 2007; Mutiti *et al*., 2010). The idea of using heat as a tracer of groundwater is an old one (e.g. Huntley, 1978), and it is based on the general observation that groundwater discharging from the ground has a contrasting heat signature compared with surrounding areas (Anderson, 2005; Pfister *et al*., 2010; Schuetz and Weiler, 2011). In northern latitudes, summer time discharge zones are cooler than the surrounding landscape, whereas winter discharge zones are warmer than the surrounding landscape. Previous studies have used this information to identify discharge zones within both freshwater (Rundquist *et al*., 1985; Banks *et al*., 1996; Conant, 2004; Tcherepanov *et al*., 2005) and marine (Wilson and Rocha, 2012) aquatic ecosystems. Only a handful of studies have used heat to identify discharge zones across terrestrial ecosystems (e.g. Bobba *et al*., 1992; Barron and Van Niel, 2009).

A significant challenge of using thermal imagery to map discharge zones on terrestrial ecosystems is the fact that land cover exerts a very strong control on surface temperatures. Therefore, the key to the success of this approach is the selection of imagery that minimizes the influence of land cover elements and maximizes the differences due to surface water – groundwater exchange (Barron and Van Niel, 2009). Ideally, images taken at night or dawn are chosen, when land cover effects on surface skin temperatures are minimized, although these effects may still be carried through from the day before (Barron and Van Niel, 2009). At higher latitudes during hemispheric winters, where solar radiation is low and vegetation is dormant, thermal differences due to land cover are minimized with respect to summer conditions. These conditions potentially make winter imagery superior in capturing thermal differences due to groundwater discharge. Bobba *et al*. (1992) showed promising results in capturing groundwater discharge zones using winter thermal imagery in a temperate watershed with different land uses, but this technique needs further validation across landscapes with varied land covers as well as the possibility of snow cover masking the groundwater signal.

The goal of this paper was to evaluate the use of thermal remote sensing for mapping groundwater discharge zones in the rolling terrain of central Alberta where J. Tóth worked out his conceptual theories of groundwater movement. This is a transitional area between the boreal and prairie ecoregions with substantial modifications of the surface for urban, agricultural and industrial uses. As a result, there is not only scientific interest to map and understand the hydrological and ecological processes at a regional scale but also interest to apply that knowledge to inform land use planning and management. Specifically, our objectives were (1) to map the location of potential groundwater discharge zones using winter thermal remote sensing and (2) to corroborate

these maps using ground-based hydrological and chemical datasets. Our remote sensing methodology is based on the assumption that discharging groundwater has a thermal signature that is distinct from non-discharge areas; that is, in winter, the ground surface in discharge areas is relatively warmer than surrounding non-discharge areas because of the moderating effect of upwelling groundwater.

METHODOLOGY

Study region

The study region is the Beaverhill subwatershed in Alberta (53.5°N, 113°W) centred on the Cooking Lake moraine located 50 km east of Edmonton and occupying a total area of 4405 km^2 (Figure 2A). The Beaverhill subwatershed contains Beaverhill Lake, an aquatic system internationally recognized for its shorebirds and waterfowl (RAMSAR convention of 1971) that drains into the North Saskatchewan River. Most of the Cooking Lake moraine is designated as part of national (Elk Island National Park) and provincial (Cooking Lake-Blackfoot Grazing, Wildlife, Provincial Recreation Area, the Ministik Bird Sanctuary, and Miquelon Lake Provincial Park) protected areas. The rest of the Beaverhill subwatershed comprises agricultural land farmed either as cropland or pastureland or is undergoing residential (e.g. Edmonton and Fort Saskatchewan) and industrial development (e.g. upgraders and refineries).

Bedrock geology is characterized by three major bedrock units including the Horseshoe Canyon Formation, the Bearpaw Formation and the Belly River Group (Figure 3A, Hamilton *et al.*, 1998). The Horseshoe Canyon Formation underlies the glacial materials over the majority of the study region. It was deposited in a marginal marine setting and is composed of fine to medium grained sediments occurring as lenticular, inter-fingered within muddy, transgressive sediments (Stein, 1979). The Bearpaw Formation consists of marine shale, with bentonite, silty shale, and discontinuous sandstone beds where it inter-fingers with the overlying Horseshoe Canyon Formation. The Bearpaw Formation's subcrop area cuts across the middle of the watershed along the eastern edge of the Cooking Lake moraine. The Belly River Group subcrops in the eastern portion of the study region and is composed also of largely marginal-marine sediments with localized areas of coarse-grained fluvial sand deposits.

The last glaciation left as many as three till sequences with variable thickness (average thickness of 21 m). The glacial till is vertically interspersed with sand and gravel lenses of glacio-fluvial origin as well as glacio-lacustrine lakebeds (Figure 3B, Hamilton *et al.*, 1998). The surficial deposits are notably thicker within the Beaverhill subwatershed than the surrounding Prairie as a result of the presence of the moraine (Barker *et al.*, 2011). Closer to the North Saskatchewan River in the north, there are sizable deposits of sand and gravel of fluvial origin.

Topography reflects glacial depositional processes and consists of hummocky, knob and kettle formations of the moraine at higher elevations surrounded by flat to rolling landscapes at lower elevations surrounding the moraine (Figure 3C). Topographic relief ranges from a high of 812 m in the moraine to a low of 586 m along the North Saskatchewan River. The soils that have formed on these glacial and fluvial deposits are mainly Orthic Gray Luvisols and Black Chernozemics.

A mixed-wood boreal forest characterizes the natural vegetation cover of the region, with prairie transition species including tree species of trembling aspen

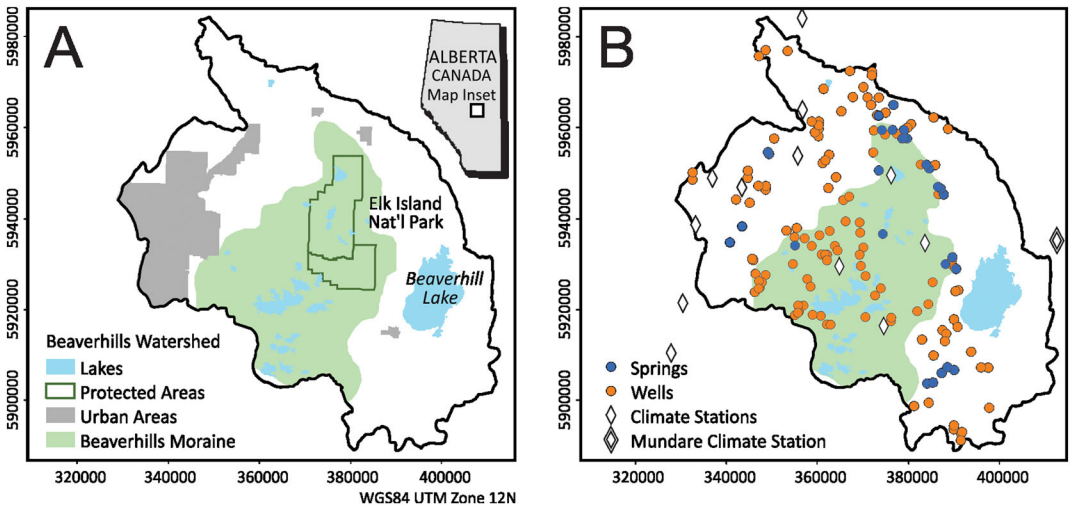

Figure 2. Maps of the Beaverhills subwatershed study region: (A) general location and main administrative and physiographic features and (B) locations of climate and hydrological measurement locations (groundwater springs and wells)

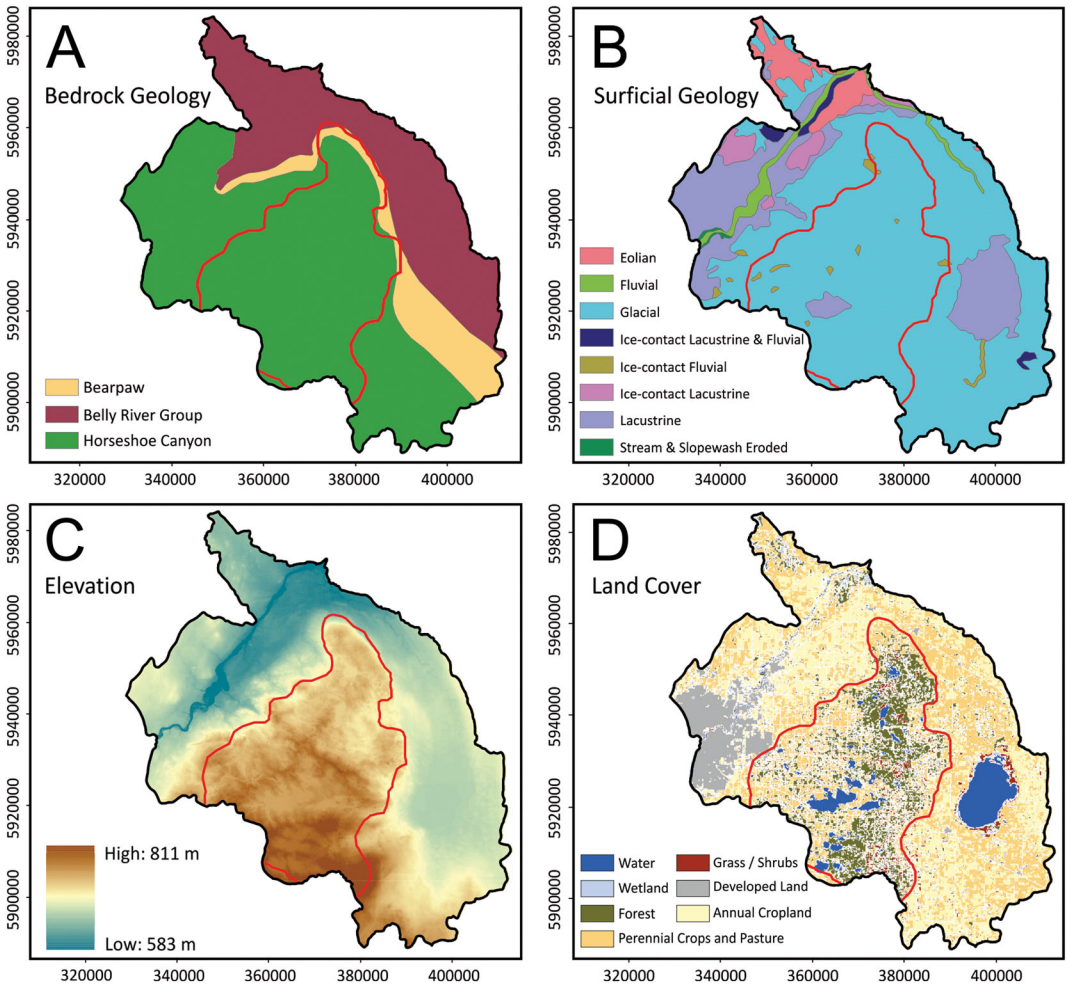

Figure 3. (A) Bedrock geology (adapted from Alberta Geological Survey Map 236, Hamilton *et al*., 1998), (B) surficial geology (adapted from Alberta Geological Survey Map 236, Hamilton *et al*., 1998), (C) elevation and (D) land use of the Beaverhills subwatershed. The red line depicts the outline of the Cooking Lake moraine

(*Populus tremuloides* Michx.), balsam poplar (*Populus balsamifera* L.) and white birch (*Betula papyrifera* Marsh) (Strong and Leggat, 1981) interspersed with grassland (Figure 3D). The lands outside of the protected areas have been farmed since the early 1900s and comprise croplands (e.g. barley, oats and canola) and pasturelands.

The climate is continental with cold winters and warm summers. Based on a 30-year (1971–2000) climate normal for Edmonton International Airport (Environment Canada Climate Normals [http://www.climate.weatheroffice.gc.ca/climate_normals/index_e.html]), average January and July temperatures are −13.5 and 15.9 °C, respectively. Annual precipitation is 483 mm, most of it (~70%) falling as rain between the months of May and September. Evaporative demand is highest during this time of year (450 mm of potential evapotranspiration [May–September]) resulting in little water left over for surface runoff. Although small as a percentage of the overall budget (~20%), winter precipitation (mostly as snow) can be an important contributor of local runoff into wetlands as the snow melts in the spring.

In terms of the surface energy balance, solar radiation reaches a minimum around the December solstice (Figure 4). This minimum in energy input by the sun is reflected in soil temperatures that reach their minimum concurrently or sometime after the solar minimum depending on the depth of measurement. Soil temperature, measured 5 cm belowground, is correlated linearly with air temperature until the snowpack forms, when soil temperatures are decoupled from the atmosphere (Figure 5). In most years, the snowpack forms by middle of December and lasts until March except for occasional mid-winter thaws (Figure 4).

The depth and spatial extent of concrete soil frost are highly variable in the study region and are highly dependent on antecedent soil moisture conditions prior to winter months, and the timing and nature of the snowpack accumulation (Metcalfe and Buttle, 1999). Wet conditions

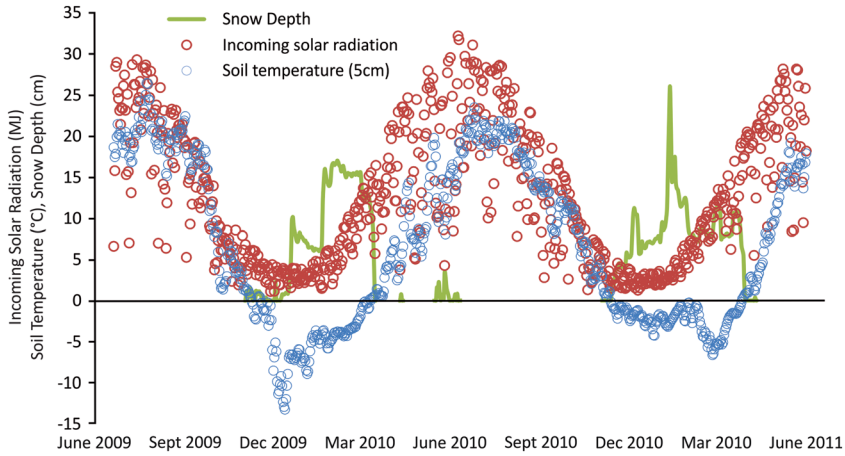

Figure 4. Two-year sequence of daily measurements in incoming solar radiation, soil temperature (5 cm below ground) and snow depth recorded at Mundare climate station [http://agriculture.alberta.ca/acis/alberta-weather-data-viewer.jsp] located near the eastern boundary of Beaverhill subwatershed (Figure 2B)

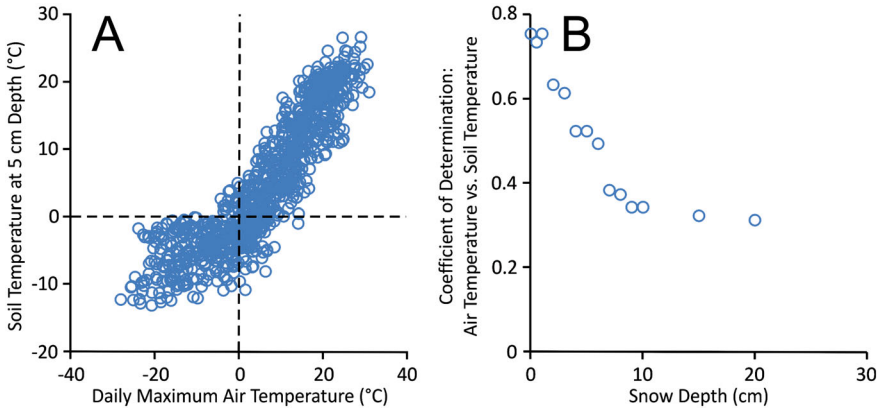

Figure 5. Coupling of air temperature with soil temperature as recorded at Mundare climate station (same data series as in Figure 4): (A) all data and (B) level of correlation for all air temperature measurements below the freezing mark and progressively discarding measurements with specific snow depth (i.e. at snow depth of 20 cm all sub-zero data points are analysed, but at zero, snow depth only measurements when there was no snow accumulation were analysed)

followed by cold temperatures and little snowpack leads to deep soil frost development. In fact, soil frost can also occur in the spring given the slow warm-up and freeze thaw cycles. However, even when conditions are optimal for significant soil frost accumulation, it is uncommon for soil frost to exceed 1 m depth from the land surface (Löfvenius *et al.*, 2003). Groundwater discharging to surface melts soil frost from below prior to air temperature driven soil frost melting. This is particularly true for areas without concrete soil frost development as the soil media has been shown to remain permeable facilitating infiltration and by extension upward exfiltration or discharge to surface (Redding and Devito, 2011).

The climate, geology and topography have collectively created a hydrological system dominated by numerous shallow lakes and wetlands on the surface and by local and regional aquifers below the surface. The relatively low precipitation rate coupled with high evaporative demand translates into minimal surface water flow volumes with only a few intermittent or slow-moving streams in the subwatershed. Precipitation patterns drive fluctuations in water levels in wetlands and lakes. For example, Beaverhill Lake has completely dried up on two occasions in the past 100 years (1945 and 2009). Given the low permeability of the till and the protected status of the moraine, there are many more lakes and wetlands on the moraine than on the surrounding agricultural regions. Although the transmission rate of water into the shallow and deeper geological deposits is slow, the moraine still serves as an important source of groundwater recharge in the area.

Regional hydrogeological flow patterns are reasonably well documented in the Beaverhill subwatershed. The flow systems within the shallow intertill aquifers are driven by local to intermediate-scale topographic features on the moraine. The regional flow pattern in the bedrock aquifers is dominated by radial flow towards the flanks of the topographic high created by the Cooking Lake

moraine. Some of this water discharges in springs and seepages along the moraine's edge, which is coincident with the edge of the Bearpaw Formation subcrop edge. As a result, it has great potential to impede vertical flow (high permeability contrast relative to the other bedrock formations and the overlying glacial materials) (Barker *et al*., 2011). This creates what are known as contact springs, which develop where sediments with relatively high permeability rest directly on a geological body with low permeability, such as clay or marine shale in the case of the Bearpaw Formation. Downward flow from the Horseshoe Canyon to the Belly River is well documented with potentiometric data showing an upward gradient across the Bearpaw Formation (Stein, 1979). The majority of the recharge occurring on the moraine enters local and intermediate scale groundwater flow systems, as only a small flux would be possible through the shale with low permeability that constitutes the Bearpaw Formation.

Mapping groundwater discharge zones using thermal imagery

Criteria for image selection. A key aspect of our methodology was the selection of appropriate imagery to map groundwater discharge zones. We used thermal images acquired by the Landsat-5 Thematic Mapper (TM) (10.45–12.4 μm) and Landsat-7 Enhanced Thematic Mapper (ETM) (10.31–12.36 μm) sensors downloaded from the USGS Landsat archives (http://glovis.usgs.gov) to complete the mapping. As a pre-screening step, images were discarded if there were clouds or haze across the study region or if there were other image anomalies. Next, we applied the following biophysical image selection criteria to the entire archive of imagery available for the study region (1983–2011) in order to identify imagery with the highest likelihood of reflecting spatial patterns of groundwater discharge.

The challenge in using sun-synchronous Landsat thermal imagery (local overpass times of about 11:30 AM) for mapping discharge zones is that the spatial pattern of surface skin temperature (which the Landsat thermal sensor measures) can be dominated by the spatial pattern in land cover each reflecting its own surface energy dynamics. In order to minimize the thermal signal of land cover, we selected imagery captured during the time of year when solar radiation is at a minimum (20 November–20 January) (Figure 4). Vegetation cover is also at a minimum during this time exposing the ground surface in most of the agriculturally dominated study region.

In addition to land cover, snow can also mask the potential groundwater discharge signal by acting as an insulating blanket where the surface temperatures of the snowpack do not necessarily reflect the temperature of the soil. Therefore, we discarded any imagery where the snowpack was greater than 5 cm deep across the study region. We arrived at this heuristic by identifying a natural break in the coefficient of determination curve testing the correlation between air and soil temperatures of the winter months, progressively discarding data points as a function of snow depth (Figure 5B).

Using these criteria, three Landsat TM thermal images were selected for further analysis (image dates: 14 January 2002, 30 November 2002 and 1 January 2003). Although previous studies used only one image for their mapping, we assumed that a more robust spatial pattern of groundwater discharge zones could be extracted if the thermal images were combined to average out the image-to-image variability in hydrological conditions as well some of the thermal signal that comes from land and snow cover effects.

Image pre-processing. We checked geometric alignment of the images by overlaying georeferenced hydrography and road layers and found all images to be well aligned across the study region. Next, we converted digital numbers recorded in the thermal images first to top-of-atmosphere (Equation 1) and then to at-sensor temperature using calibration constants (Equation 2) (Markham and Barker, 1986; Barsi *et al*., 2003).

$$L_{\text{cal}} = \text{Gain}^{*}Q_{\text{cal}} + \text{Offset} \tag{1}$$

where L_{cal} is calibrated radiance in W/(m^2·sr·μm) Gain ((W/(m^2 · sr · μm))/counts) and Offset (W/(m^2·sr·μm)) are rescaling factors provided in Landsat image metadata, and Q_{cal} is the digital number of the thermal image.

$$T = K_2/[\ln(K_1/L_{\text{cal}} + 1)] \tag{2}$$

where T is effective at-sensor temperature in K assuming emissivity of one; K_2 is calibration constant 2 in units of K; K_1 is calibration constant 1 in units of W/(m^2·sr·μm); and L_{cal} is calibrated radiance in units of W/(m^2·sr·μm). We used the values of 607.76 and 1260.56 for K_1 and K_2, respectively (Markham and Barker, 1986). At-sensor temperatures were converted from units of K to °C.

Each image was captured under stable atmospheric conditions. For this reason, we assumed that atmospheric effects were uniform. Further, we assumed that surface effects were spatially uniform and that conversion to absolute surface temperatures was not necessary, as the focus of the study was on extracting and analysing the spatial pattern of surface temperature. As a check, we compared average at-sensor temperature (across the study region) and average hourly air temperature at all climate stations within the study region at the time of acquisition and found a near one-to-one relationship (Figure 6).

Discharge zone mapping. The three images were combined into one thermal map by computing an average

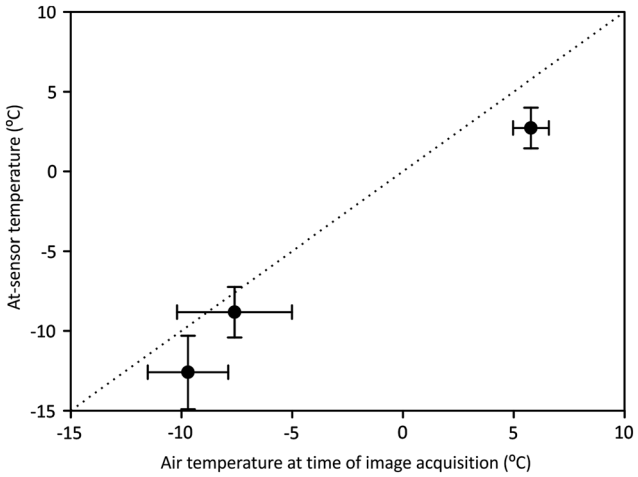

Figure 6. The relationship between air temperature as measured by weather stations (Figure 2B) and at-sensor temperature measured by satellite. The dashed line represents a 1 : 1 relationship

at-sensor temperature (Figure 7A). We masked out urban areas, given the strong effect of the urban heat island, as well as open water areas, due to the different thermal signature of ice (or open water) compared with land temperatures. The temperature range in this combined thermal map was −12.2 to −1.9 °C with a mean of −6.2 °C and standard deviation of 1.4 °C. We also computed the standard deviation and coefficient of variation of each pixel of the three images to identify areas that changed the most between the three images (Figure 7B and 6C).

Next, we developed a simple 2-class classification scheme to classify the thermal map into discharge and non-discharge zones. A known area of strong discharge was selected based on local accounts of springs and seepages as well as the general location of headwater area of streams based on a hydrography layer. Image values of the averaged thermal map along a transect were digitally extracted from a topographic high in the moraine to stretch across the potential discharge area and beyond (Figure 8A, B). A threshold between discharge and non-discharge classes was identified by looking for abrupt changes in temperature along a part of the transect with similar topography and land cover. Closer to the northern end of the transect, the temperature changes significantly (Δ3 °C) over a 3-km stretch of flat, agricultural terrain; the mid-point of this large temperature gradient was used as the classification threshold between discharge and non-discharge areas (Figure 8C). After applying the selected threshold to the averaged thermal image, a 3 × 3 majority filter was used to smooth the classified image. Hereafter, we refer to the remote sensing derived classified discharge/non-discharge map as the classified discharge map (Figure 7A).

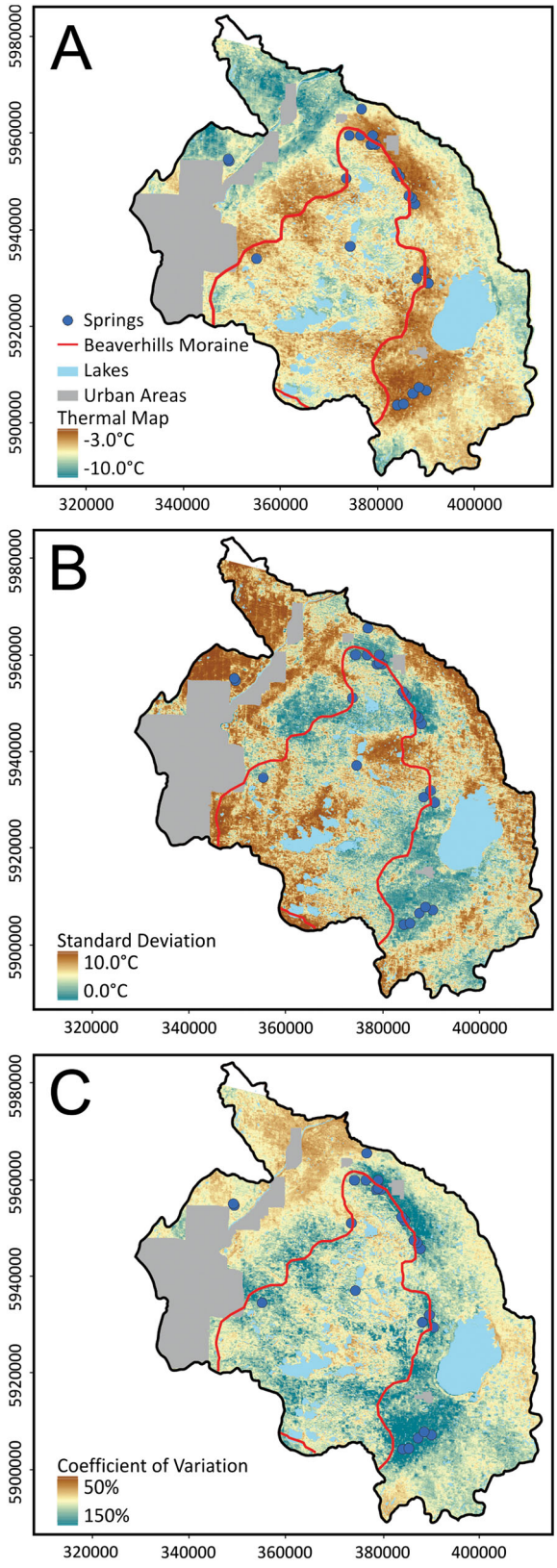

Figure 7. Thermal composite maps (A) based on an average, (B) standard deviation and (C) coefficient of variation of three winter Landsat thermal images. Areas of brown hues in map (A) are warmer areas potentially corresponding to groundwater discharge zones

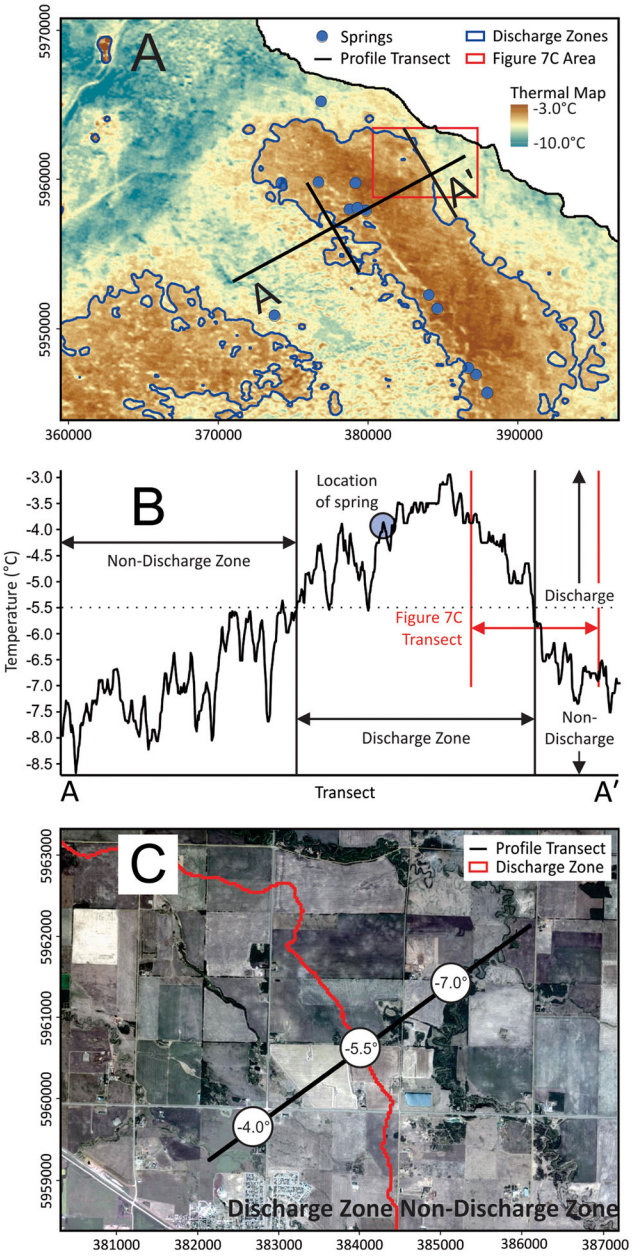

Figure 8. Visual depiction of the method for selecting class boundary of discharge and non-discharge zones from the thermal composite map: (A) a cross-section was identified based on local knowledge of springs, (B) the cross-sectional profile of temperature was mapped along the selected path and (C) an area of abrupt change in temperature was selected (red box in A)

Corroboration of ground-based and remotely sensed discharge map

Hydrological evidence: spring locations and water table depth. We used two hydrological sources of corroborating evidence to assess the accuracy of the classified discharge map: (1) spring locations mapped by the Alberta Geological Survey (AGS) (http://www.ags.gov.ab.ca/publications/abstracts/DIG_2009_0002.html) and (2) static water-level depth measured in shallow wells (<10 m bgs [below ground surface]) extracted from the Alberta Water Well Information Database (AWWID; http://environment.alberta.ca/01314.html) (Figure 2B). It was assumed that the static water levels of shallow wells would reflect the position of the water table. The presence/absence of springs within the two zones (discharge and non-discharge) was determined; the expectation was that all springs would fall within discharge zones. The statistically significant difference in at-sensor temperatures between spring influenced areas (120 m buffer around spring locations) and non-spring influenced areas were assessed. Using the static water levels, non-parametric Mann–Whitney U Tests were conducted to test the hypothesis that there were statistically significant ($p < 0.05$) differences in water-table depth between discharge and non-discharge zones; we predicted that discharge zones would have shallower (i.e. closer to the ground surface) water tables.

Chemical evidence: water-well chemistry. All available chemistry data measured in shallow wells (<10 m bgs) from the AWWID were used to test for differences in often used tracers of groundwater flow including the concentrations of TDS, sodium (Na), chloride (Cl), calcium (Ca), and magnesium (Mg) as well as electrical conductivity (EC). Non-parametric Mann–Whitney U Tests were conducted to test the hypothesis that there were statistically significant ($p < 0.05$) differences in chemical signatures between discharge and non-discharge zones; we predicted that discharge zones would have higher concentrations of these tracers than non-discharge zones reflecting a longer contact period with the substrate (Devito *et al.*, 2000).

RESULTS

The thermally classified map of groundwater discharge zones is presented in Figure 9. Discharge zones occurred in topographically low areas but not necessarily the lowest areas. Discharge zones were located on the slopes and at the bottom of the slopes surrounding the moraine, especially the northeastern flank of the moraine and the area surrounding the southwestern tip of Beaverhill Lake.

Hydrological data provided independent support for the thermally classified discharge map. Of the 26 springs located within the non-urban portion of the Beaverhill subwatershed according to the AGS-springs database, 22 springs fell within the classified discharge zones, corresponding to an 85% accuracy of predicting springs as part of discharge zones. One other spring was located within 200 m of the classified map boundary. Comparison of averaged at-sensor temperatures (Figure 9 inset)

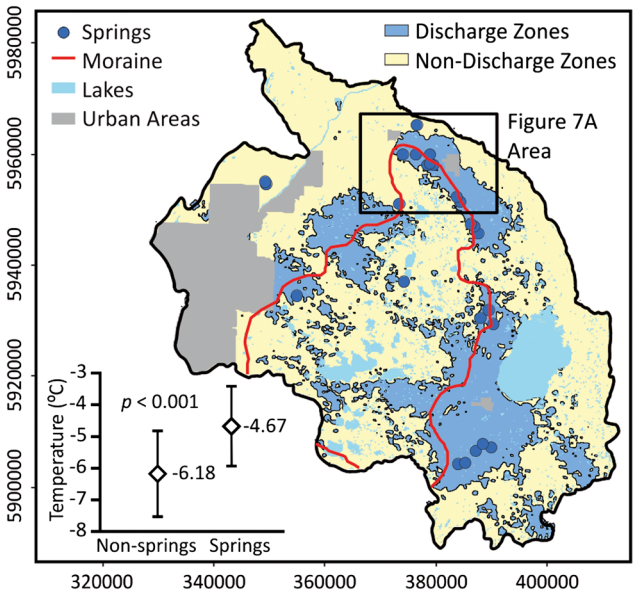

Figure 9. Classified groundwater discharge map inferred from satellite thermal remote sensing and conceptual understanding of groundwater movement. The inset figure shows the mean and standard deviation of thermal composite map values within and outside of 120 m buffers of spring locations

between spring-influenced (i.e. 120 m buffer around spring locations) and non-spring areas revealed statistically significant differences, where spring-influenced areas (−4.7 °C ± 1.3 °C) were about 1.5 °C warmer than non-spring influenced areas (−6.2 °C ± 1.4 °C) ($p < 0.001$) (Figure 9 inset). Static water levels were slightly closer to the ground surface in discharge areas (as expected); however, the difference was significant only at $p < 0.1$ (Table I).

Hydrochemical data provided further support for the thermally classified discharge map. EC, Na and TDS as measured in groundwater wells showed statistically higher averages within discharge zones than non-discharge zones ($p < 0.05$) (Table I). For example, TDS increased in value from 789 mg/l in non-discharge zones to 1001 mg/l in discharge zones, whereas EC increased in value from 1150 µS/cm in non-discharge zones to 1507 µS/cm in discharge zones.

In summary, the classified discharge map was corroborated by topographic, geologic, hydrological and chemical signals of groundwater discharge zones. The discharge zones as identified by classification of the Landsat images were located in topographic low areas and areas where the geology would also predict movement of water towards the surface. Most of the springs in the Beaverhill subwatershed were located within mapped discharge zones and TDS showed higher concentrations in mapped discharge zones as opposed to non-discharge zones.

DISCUSSION

Mapping of groundwater discharge zones at the watershed scale is a challenge, particularly in data sparse regions. This challenge exists because the measurements with which groundwater flow direction and rate can be made directly and accurately (i.e. piezometer nests measuring hydraulic head at different depths) are expensive, ecologically intrusive and impractical. As a result, discharge patterns mapped using methodologies applicable to broad spatial scales, including remote sensing analysis, which do not directly measure groundwater flow, need to be corroborated by multiple lines of evidence that can be used to infer groundwater movement (Barron and Van Niel, 2009).

In his classic ground-based study of groundwater discharge (and recharge) mapping, Tóth (1966) identified two types of evidence for the corroboration of discharge patterns: (1) features pertaining to the environment and

Table I. Median well-based water level and well-based chemical tracers of groundwater movement between discharge and non-discharge zones of the classified discharge map (numbers in brackets signify the number of wells in each class)

Parameter	Units	Non-discharge	Discharge	Mann–Whitney U	*p*-value
Water level	m	3.96 [73]	3.48 [43]	1276	0.093
Ca	mg/l	101.0 [68]	87.0 [40]	1207.5	0.333
Cl	mg/l	11.0 [69]	14.0 [45]	1513	0.821
Mg	mg/l	32.0 [67]	29.5 [38]	1137	0.366
Na	mg/l	51.0 [52]	230.5 [36]	**624.5**	**0.008**
EC	µS/cm	1150.0 [71]	1507.5 [46]	**1097**	**0.003**
Total dissolved solids	mg/l	789.0 [75]	1001.5 [46]	**1248.5**	**0.011**

(2) features pertaining to water. Environmental features include climate, topography and geology. Features pertaining to water include *actual* and *associated* aspects of presence (or absence) and of the physical and chemical properties of water. Actual aspects of water include springs, seepages, groundwater levels, flowing wells, chemical quality of water (i.e. distribution of the chemical components) and physical quality of water (e.g. temperature and turbidity), whereas associated aspects include natural vegetation, salt precipitates, 'burnt crops', soap holes, moist depressions, dry depressions, man-made objects and local reports.

In this 'thermal remote sensing' study, environmental, hydrological and hydrochemical evidence were used to corroborate the thermally classified discharge map. It needs to be emphasized that this map reflects the locations of potential discharge zones and does not convey information about rates of flow. Our results indicated that the map reflected patterns of discharge zones that would also be inferred from ground-based evidence.

Environmental data (topography and geology) provide a qualitative indication that the classified discharge map reflects realistic patterns of discharge zones. Discharge zones occurred at breaks in slope at the edge of a significant topographic feature (Cooking Lake moraine) and also coincided with a geological formation (Bearpaw) with a very low permeability. The Bearpaw Formation separates artesian hydraulic head values from the land surface and also exerts potentially strong effects of topographic discharge through secondary porosity (e.g. macro-pores, rootlets, abandoned root channels and fractures). The lack of discharge zones in the North Saskatchewan River valley (in the northern portion of the watershed where one may expect topographically driven discharge to occur) coincides with highly permeable sands and gravels (Figure 3A,B). However, environmental data are only useful as a general assessment tool for predicting the potential for discharge.

Hydrological and hydrochemical data provided a quantitative corroboration of our thermally derived discharge map. The static water table levels measured in shallow wells were closer to the surface in discharge zones, as expected by theory (Tóth, 1966), but only significant at a p of less than 0.1 (Table I). This weaker than expected result could be partly due to the limitation of the dataset, which includes well data collected across a wide temporal range representing different hydrological conditions. Alternatively, the lack of stronger differences in static water levels could be due to a combination of permeability and water availability, where more abundant surface water on the moraine (site of focused recharge through wetlands and lakes) and a low permeability till means perched water tables are close to the surface.

Much stronger ground-based support for the classified map of discharge zones was provided by the spatial analysis of the occurrence of springs. These are areas where groundwater is actively discharging onto the surface because of strong upward flow. AGS mapped 26 springs within the Beaverhill subwatershed, all but three of them located at the edge of the Cooking Lake moraine. Many (but not all) of these springs surrounding the moraine also coincided with the subcropping of the Bearpaw Formation. In terms of our mapping, 22 of 26 (85%) of the springs were located within discharge zones giving strong corroborating evidence. Unfortunately, very little flow rate data are available from the springs documented in the area. The limited quantitative data available shows a significant range in flow rates from <0.02 l/s to 0.2 l/s. However, many of the springs identified by the AGS that fall in the discharge zones are identified as soap holes or 'quick-sand' with anomalously high pore pressure in the surface substrate suggesting spring permanence or perennial upward flow of groundwater. The springs with undocumented flow rates are likely to have low, intermittent or variable flow rates, which could perhaps explain why some of the springs were not captured by the discharge zones of the thermal map.

Chemical tracers of groundwater flow as measured in groundwater wells showed significant statistical differences between discharge zones and those outside of them (Table I). Discharge zones had higher concentrations of TDS and sodium as well as higher EC, supporting the well-established notion that predicts higher degrees of mineralization as a result of longer time spent by water in the groundwater flow system (Tóth, 1999; Martin and Soranno, 2006). Tóth (1966) also documented higher TDS in discharge zones in a similar environment, located about 200 km to the south of our study region. More recent studies looking at lake water and its relation to flow systems have also documented an increase in Ca, Mg, Cl, Na as well as TDS and EC as lake order or lake groundwater position increased (e.g. Martin and Soranno, 2006). Devito *et al.* (2000), focusing on boreal watersheds located to the north by about 300 km of our study region, found an increase in the concentration of conservative tracers of groundwater in lakes which are located in discharge rather than recharge zones. Flowpath length may be confounded by differences in the composition of the substrate. Our dataset of well chemistry did show some differences in TDS and EC based on bedrock geology but not in a way that would confuse our hydrogeological interpretation. Belly River formation showed statistically lower TDS and EC values than the Bearpaw and Horseshoe (Figure 3A). In terms of surficial geology, only the minor classes (e.g. fluvial, eolian and ice-contact lacustrine) showed significantly

different TDS and EC values (Figure 3B). The majority classes of glacial and lacustrine showed similar values in TDS and EC making our assumption of using these chemical signals as interpreters of groundwater flowpath length more valid.

This study clearly shows that thermal remote sensing is capable of capturing spatial patterns of discharge zones at a regional scale. This discharge zone mapping method works because the thermal signature of discharge zones is different from the surrounding non-discharge zones, especially during the coldest part of the year when vegetation effects on surface temperatures are minimized. Although we applied stringent image selection criteria to minimize the effects of land and snow cover, it is possible that the final classified map retained a vegetation signal especially due to coniferous forests located on the moraine.

This study also highlights the importance of basic hydrological, hydrogeological and chemical data collection programs and perhaps expanding the geophysical (e.g. ground-penetrating radar) data collection, which can be used to calibrate regional scale mapping. In terms of applying these techniques in other places in North America and around the world, it needs to be stressed that the thermal mapping used here is only applicable in cold climates where the combination of low solar radiation and minimal vegetation cover in the winter minimize land cover effects and allow ground heat to influence surface temperatures. The window of opportunity to acquire the appropriate imagery is small, but the vast USGS archive and the fairly stationary groundwater signal make it probable to find at least a few images for mapping. We used an averaging approach to factor out more of the unwanted signal due to residual snow and vegetation effects, but our perusal of the individual images (now shown) made it clear that even one, carefully selected image, could be used for the type of mapping we advocate for in this paper.

CONCLUSION

There is significant interest in mapping groundwater discharge patterns for scientific and management related issues, such as understanding the effect of discharging water on ecosystem processes as well as predicting contaminant transport processes. There is a need to understand and manage the groundwater surface water system as one system, and therefore, information gathering techniques are needed that can do the job at broad spatial scales. The thermal remote sensing mapping technique employed in this study provides invaluable first-order information on groundwater discharge zones. Not only does it provide useful information for more detailed field or modelling investigations, but knowledge of these zones may also help explain hydrological and ecological dynamics of data sparse regions of northern human settled areas.

ACKNOWLEDGEMENTS

GZS was funded by an NSERC Post-doctoral fellowship. The research was funded by an Alberta Water Research Institute Grant to IFC and SEB, the Alberta Geological Survey - Provincial Groundwater Inventory Program and an NSERC Discovery Grant to IFC. The authors gratefully acknowledge USGS for providing Landsat images. The views expressed herein are those of the authors, and may or may not coincide with policies or mandates of these two institutions. The authors would also like to thank Johnston Miller, David Aldred and two anonymous reviewers for providing insightful comments which significantly improved the quality of the manuscript.

REFERENCES

Anderson MP. 2005. Heat as a ground water tracer. *Ground Water* **43**: 951–968.

Banks WSL, Paylor RL, Hughes WB. 1996. Using thermal-infrared imagery to delineate ground-water discharge. *Ground Water* **34**: 434–443.

Barker AA, Riddell JTF, Slattery SR, Andriashek LD, Moktan H, Wallace S, Lyster S, Jean G, Huff GF, Stewart SA, Lemay TG. 2011. Edmonton–Calgary corridor groundwater atlas; Energy Resources Conservation Board, ERCB/AGS Information Series 140, 90 pp.

Barron O, Van Niel T. 2009. Application of thermal remote sensing to delineate groundwater discharge zones. *International Journal of Water* **5**: 109–124.

Barsi JA, Schott JR, Palluconi FD, Helder DL, Hook SJ, Markham BL, Chander G, O'Donnell EM. 2003. Landsat TM and ETM + thermal band calibration. *Canadian Journal of Remote Sensing* **29**: 141–153.

Batelaan O, De Smedt F, Triest L. 2003. Regional groundwater discharge: phreatophyte mapping, groundwater modelling and impact analysis of land-use change. *Journal of Hydrology* **275**: 86–108.

Becker MW. 2006. Potential for satellite remote sensing of ground water. *Ground Water* **44**: 306–318.

Bobba AG, Bukata RP, Jerome JH. 1992. Digitally processed satellite data as a tool in detecting potential groundwater-flow systems. *Journal of Hydrology* **131**: 25–62.

Brunke M, Gonser T. 1997. The ecological significance of exchange processes between rivers and groundwater. *Freshwater Biology* **37**: 1–33.

Cartwright K. 1974. Tracing shallow groundwater systems by soil temperatures. *Water Resources Research* **10**: 874–855.

Conant B. 2004. Delineating and quantifying ground water discharge zones using streambed temperatures. *Ground Water* **42**: 243–257.

Curry RA, Noakes DLG. 1995. Groundwater and the selection of spawning sites by brook trout (Salvelinus fontinalis). *Canadian Journal of Fisheries and Aquatic Sciences* **52**: 1733–1740.

Devito KJ, Creed IF, Rothwell RL, Prepas EE. 2000. Landscape controls on phosphorus loading to boreal lakes: implications for the potential impacts of forest harvesting. *Canadian Journal of Fisheries and Aquatic Sciences* **57**: 1977–1984.

Euliss N, LaBaugh J, Frederickson L, Mushet D, Laubhan M, Swanson G, Winter T, Rosenberry D, Nelson R. 2004. The wetland continuum: a conceptual framework for interpreting biological studies. *Wetlands* **24**: 448–458.

Hamilton WN, Langenberg CW, Price MC, Chao DK. 1998. *Geologic Map of Alberta*. Alberta Geological Society. http://www.ags.gov.ab.ca/publications/abstracts/MAP_236.html. Date accessed: Jan 01, 2013.

Huntley D. 1978. On the detection of shallow aquifers using thermal infrared imagery. *Water Resources Research* **14**: 1075–1083.

Levine JB, Salvucci GD. 1999. Equilibrium analysis of groundwater-vadose zone interactions and the resulting spatial distribution of hydrologic fluxes across a Canadian prairie. *Water Resources Research* **35**: 1369–1383.

Löfvenius MO, Kluge M, Lundmark T. 2003. Snow and soil frost depth in two types of shelterwood and a clearcut area. *Scandinavian Journal of Forest Research* **18**: 54–63.

Markham BL, Barker JL. 1986. Landsat MSS and TM post-calibration dynamic ranges, exoatmospheric reflectances and at-satellite temperatures. Earth Observation Satellite Co., Lanham, MD, Landsat Tech. Note 1.

Martin SL, Soranno PA. 2006. Lake landscape position: relationships to hydrologic connectivity and landscape features. *Limnology & Oceanography* **51**: 801–814.

Metcalfe RA, Buttle JM. 1999. Semi-distributed water balance dynamics in a small boreal forest basin. *Journal of Hydrology* **226**: 66–87.

Mutiti S, Levy J, Mutiti C, Gaturu NS. 2010. Assessing ground water development potential using Landsat imagery. *Ground Water* **48**: 295–305.

Neufeld DA. 2000. An ecosystem approach to planning for groundwater: the case of Waterloo Region, Ontario, Canada. *Hydrogeology Journal* **8**: 239–250.

O'Connor D. 2002. *Report of the Walkerton Commission of Inquiry*, Publications Ontario.

Pfister L, McDonell JJ, Hissler C, Hoffmann L. 2010. Ground-based thermal imagery as a simple, practical tool for mapping saturated area connectivity and dynamics. *Hydrological Processes* **24**: 3123–3132.

Pires M. 2004. Watershed protection for a world city: the case of New York. *Land Use Policy* **21**: 161–175.

Power G, Brown RS, Imhof JG. 1999. Groundwater and fish – insights from northern North America. *Hydrological Processes* **13**: 401–422.

Redding T, Devito K. 2011. Aspect and soil textural controls on snowmelt runoff on forested Boreal Plain hillslopes. *Hydrology Research* **42**: 250–267.

Rundquist D, Murray G, Queen L. 1985. Airborne thermal mapping of a "flow-through" lake in the Nebraska Sandhills. *Water Resources Bulletin*, **21**: 989–994.

Schuetz T, Weiler M. 2011. Quantification of localized groundwater inflow into streams using ground-based infrared thermography. *Geophysical Research Letters* **38**: L03401. doi: 10.1029/2010GL046198.

Soulsby C, Malcolm IA, Tetzlaff D, Youngson AF. 2009. Seasonal and inter-annual variability in hyporheic water quality revealed by continuous monitoring in a salmon spawning stream. *River Research and Applications* **25**: 1304–1319.

Stein R. 1979. Hydrogeology of the Edmonton area (southeast segment), Alberta, *Earth Sciences Report 79*, Alberta Research Council, 16pp.

Strong WL, Leggat KR. 1981. *Ecoregions of Alberta, Alberta Environment Natural Resources*. Resource Evaluation Planning Division: Edmonton.

Tcherepanov EN, Zlotnik VA, Henebry GM. 2005. Using Landsat thermal imagery and GIS for identification of groundwater discharge into shallow groundwater-dominated lakes. *International Journal of Remote Sensing* **26**: 3649–3661.

Tóth J. 1963. A theoretical analysis of groundwater flow in small drainage basins. *Journal of Geophysical Research* **68**: 4795–4812.

Tóth J. 1966. Mapping and interpretation of field phenomena for groundwater reconnaissance in a prairie environment, Alberta, Canada. *International Association of Scientific Hydrology Bulletin* **16**: 20–68.

Tóth J. 1971. Groundwater discharge: a common generator of diverse geologic and morphologic phenomena. *International Association of Scientific Hydrology Bulletin* **16**: 7–24.

Tweed SO, Leblanc M, Webb JA, Lubczynski MW. 2007. Remote sensing and GIS for mapping groundwater recharge and discharge areas in salinity prone catchments, southeastern Australia. *Hydrogeology Journal* **15**: 75–96.

Tóth J. 1999. Groundwater as a geological agent: an overview of the causes, processes, and manifestations. *Hydrogeology Journal* **7**: 1–14.

Whiteman MI, Seymour KJ, van Wonderen JJ, Maginness CH, Hulme PJ, Grout MW, Farrell RP. 2012. Start, development and status of the regulator-led national groundwater resources modelling programme in England and Wales. In *Groundwater Resources Modelling: A Case Study from the UK*, Shepley MG, Whiteman MI, Hulme PJ, Grout MW (eds). Geological Society: London; 19–37.

Wilson J, Rocha C. 2012. Regional scale assessment of Submarine Groundwater Discharge in Ireland combining medium resolution satellite imagery and geochemical tracing techniques. *Remote Sensing of Environment* **119**: 21–34.

Winter TC, Harvey JW, Franke OL, Alley WM. 1998. *Ground Water and Surface Water a Single Resource*. US Geological Survey: Denver, CO.

